

# On the Unique Solution of Planet and Star Parameters from an Extrasolar Planet Transit Light Curve

S. Seager<sup>1</sup> and G. Mallén-Ornelas<sup>2</sup>

## ABSTRACT

There is a unique solution of the planet and star parameters from a planet transit light curve with two or more transits if the planet has a circular orbit and the light curve is observed in a band pass where limb darkening is negligible. The existence of this unique solution is very useful for current planet transit surveys for several reasons. First, there is an analytic solution that allows a quick parameter estimate, in particular of  $R_p$ . Second, the stellar density can be uniquely derived from the transit light curve alone. The stellar density can be used to immediately rule out a giant star (and hence a much larger than planetary companion) and can also be used to put an upper limit on the stellar and planet radius even considering slightly evolved stars. Third, the presence of an additional fully blended star that contaminates an eclipsing system to mimic a planet transit can be largely ruled out from the transit light curve given a spectral type for the central star. Fourth, the period can be estimated from a single-transit light curve and a measured spectral type. All of these applications can be used to select the best planet transit candidates for mass determination by radial velocity follow-up. To use these applications in practice, the photometric precision and time sampling of the light curve must be high (better than 0.005 mag precision and 5 minute time sampling).

## 1. Introduction

Planet transit searches promise to be the next big step forward for extrasolar planet detection and characterization. Every transiting planet discovered will have a measured radius, which will provide constraints on planet composition, evolution, and migration history. Together with radial velocity measurements, the absolute mass of every transiting planet will be determined. Transiting planets can be discovered around distant stars and in a variety of environments. Due to their special geometry many follow-up observations of transiting planets are possible, such as atmosphere transmission spectroscopy (note the first extrasolar planet atmosphere detection by Charbonneau et al. 2002), search for moons and rings (Brown et al. 2001), and detection of oblateness and the corresponding constraint on rotation rate (Seager & Hui 2002). Although no planet candidates discovered by the transit method have yet been confirmed by mass measurements, many searches are currently ongoing. The OGLE-III planet search (Udalski et al. 2002) has observed numerous high-precision transit light curves from objects with small radii, including several potential planets. The EXPLORE search (Mallén-Ornelas et al. 2002; Yee et al. in preparation) has four potential planet candidates based on both photometric light curves and follow-up radial velocity measurements (Mallén-Ornelas et al., in preparation). The Vulcan planet search (Borucki et al. 2001) has some published results on transit candidates that, with radial velocity measurements, were determined to be eclipsing binary stars (Jenkins, Caldwell, & Borucki 2002).

---

<sup>1</sup>Institute for Advanced Study, Einstein Drive, Princeton, NJ, 08540; seager@ias.edu

<sup>2</sup>Princeton University Observatory, Peyton Hall, Princeton NJ, 08544-0001 and Departamento de Astronomía y Astrofísica, Pontificia Universidad Católica de Chile, Casilla 306, Santiago 22, Chile; mallen@astro.princeton.edu

Follow-up mass determination by radial velocity measurements are needed for planet transit candidates because late M dwarfs ( $M \geq 80M_J$ ), brown dwarfs ( $13M_J < M < 80M_J$ ), and gas giant planets ( $M \leq 13M_J$ ) are all of similar sizes. This is due to a coincidental balance between Coulomb forces (which cause  $R \sim M^{1/3}$ ) and electron degeneracy pressure (which causes  $R \sim M^{-1/3}$ ). A high yield of confirmed planets from a list of planet candidates considered for mass follow-up is important, especially for planet searches with faint stars (e.g., fainter than 13th magnitude) which require relatively long exposures on 8-m class telescopes (e.g., 20–30 mins per star for a single radial velocity measurement). Hence understanding the transit light curves before follow-up can be crucial if a given project has a large number of planet transit candidates.

An analytical solution is always worthwhile to understand the general properties of a given physical system in an intuitive form. This is the case even when numerical fits are in practice the best way to determine the system parameters. In the case of a planet transit light curve we found that there is a unique solution for the five parameters stellar mass  $M_*$ , stellar radius  $R_*$ , companion radius  $R_p$ , orbital distance  $a$ , and orbital inclination  $i$ , under some important assumptions. This unique solution has several interesting applications — especially when the photometric precision and time sampling are high — including selection of the best planet candidates for follow-up mass measurements. Selection of the best candidates is especially important if the tendency for planets with small orbital distances to have low mass (Zucker & Mazeh 2002) — and hence low radial velocity amplitudes — is generally true. In this case, on average, more effort to detect the planet mass via radial velocity variations of the parent star will be needed since the primary star’s radial velocity amplitude scales linearly with planet mass.

The unique solution to a light curve with two or more transits was first mentioned in Mallén-Ornelas et al. (2002) where an approximate set of equations and a short description were presented. Sackett (1995) briefly touches on the unique solution by outlining parameter derivation with a known stellar spectral type, including a mention of period determination from a single transit. We begin this paper by describing the assumptions necessary to determine the unique solution in §2. In §3, for the first time, we present both the general set of equations that describe a planet transit light curve and their analytic solution. We discuss the errors in the parameters, and hence the limiting photometric precision and time sampling needed for the applications outlined in this paper in §4. The complications of limb-darkening are discussed in §5. In §6 we present four interesting applications that are made possible by the unique solution to the planet transit light curve. §7 concludes this paper with a summary.

## 2. Assumptions

The unique determination of the stellar mass  $M_*$ , stellar radius  $R_*$ , companion radius  $R_p$ , orbital distance  $a$ , and orbital inclination  $i$  from a light curve with two or more eclipses requires the following assumptions:

- The planet orbit is circular;
- $M_p \ll M_*$  and the companion is dark compared to the central star;
- The stellar mass-radius relation is known;
- The light comes from a single star, rather than from two or more blended stars.

The unique determination also requires the light curve to fulfill the following conditions:

- The eclipses have flat bottoms which implies that the companion is fully superimposed on the central star’s disk;
- The period can be derived from the light curve (e.g., the two observed eclipses are consecutive).

The first three assumptions are all reasonable for current extrasolar planet transit searches. Circular orbits are expected for short-period planets due to their short tidal circularization timescale, and all but one of the currently known short-period planets ( $< 4.3$  days) have eccentricities consistent with zero<sup>3</sup>. All current ground-based transit searches are searching for or expecting to find mostly short-period planets which have the highest geometric probability to show transits. The stellar mass-radius relation is reasonably well-known for each separate class of stars (e.g., main sequence), and as we show later, the mass-radius relation is not needed for a derivation of all parameters. The only assumption that has a significant chance of being wrong is the presence of a blended star (e.g., from a physical stellar companion); this situation and its possible identification are discussed in §6. The required conditions listed above are also all reasonable. Flat-bottomed transits will appear in a band pass where limb darkening is negligible, such as *I*-band. Several transit surveys are using *I*-band including OGLE-III (Udalski et al. 2002), EXPLORE (Mallén-Ornelas et al. 2002), and STEPPS (C. J. Burke et al., in preparation), and follow-up measurements for other surveys could be taken in *I*-band or in even a redder color in order to exploit the unique solution discussed in this paper. (See §5 for a discussion of limb darkening). For the rest of the paper we will work under the assumptions and conditions listed above, unless otherwise stated.

### 3. The Equations and Solution for a Light Curve with Two or More Transits

#### 3.1. The General System of Equations

There are five equations that completely describe the planet transit light curve. The first three equations (equations (1)–(3)) describe the geometry of the transit in terms of transit depth, transit shape, and transit duration (see Figure 1). For a planet transit light curve which is due to two spheres passing in front of each other, the geometry is relatively straightforward (see Sackett (1995) for a derivation of the transit duration equation (3)). Here we parameterize the transit shape by both  $t_T$ , the total transit duration (first to fourth contact), and by  $t_F$ , the duration of the transit completely inside ingress and egress (second to third contact). The three geometrical equations that describe the transit light curve depend on four observables: the period  $P$ , the transit depth  $\Delta F$ ,  $t_F$ , and  $t_T$ . See Figure 1 for an illustrative definition of  $\Delta F$ ,  $t_F$ , and  $t_T$ . In addition to the three geometrical equations there are two physical equations (equations (4)–(5)), Kepler’s Third Law and the stellar mass-radius relation. It is these physical equations that break the degeneracy of the mathematical description of two spheres passing in front of each other, by setting a physical scale. It is this physical scale, together with the geometrical description, that allows the unique solution.

The equations are: the transit depth,  $\Delta F$ , with  $F$  defined as the total observed flux,

$$\Delta F \equiv \frac{F_{no\ transit} - F_{transit}}{F_{no\ transit}} = \left(\frac{R_p}{R_*}\right)^2; \quad (1)$$

the transit shape, described by the ratio of the duration of the “flat part” of the transit ( $t_F$ ) to the total

---

<sup>3</sup>Extrasolar Planets Encyclopaedia <http://cfa-www.harvard.edu/planets/>

transit duration ( $t_T$ )

$$\frac{t_F}{t_T} = \frac{\arcsin\left(\frac{R_*}{a} \left[ \frac{\left(1 - \frac{R_p}{R_*}\right)^2 - \left(\frac{a}{R_*} \cos i\right)^2}{1 - \cos^2 i}\right]^{1/2}\right)}{\arcsin\left(\frac{R_*}{a} \left[ \frac{\left(1 + \frac{R_p}{R_*}\right)^2 - \left(\frac{a}{R_*} \cos i\right)^2}{1 - \cos^2 i}\right]^{1/2}\right)}; \quad (2)$$

the total transit duration

$$t_T = \frac{P}{\pi} \arcsin\left(\frac{R_*}{a} \left[ \frac{\left(1 + \frac{R_p}{R_*}\right)^2 - \left(\frac{a}{R_*} \cos i\right)^2}{1 - \cos^2 i}\right]^{1/2}\right); \quad (3)$$

Kepler's Third Law, assuming a circular orbit, where  $G$  is the universal gravitational constant and  $M_p$  the planet mass,

$$P^2 = \frac{4\pi^2 a^3}{G(M_* + M_p)}; \quad (4)$$

and the stellar mass radius relation,

$$R_* = kM_*^x, \quad (5)$$

where  $k$  is a constant coefficient for each stellar sequence (main sequence, giants, etc.) and  $x$  describes the power law of the sequence (e.g.,  $x \simeq 0.8$  for F–K main sequence stars (Cox 2000)).

## 3.2. Analytical Solution

### 3.2.1. Four Parameters Derivable from Observables

We ultimately wish to solve for the five unknown parameters  $M_*$ ,  $R_*$ ,  $a$ ,  $i$ , and  $R_p$  from the five equations above. It is first useful to note that four combinations of physical parameters can be found directly from the observables ( $\Delta F$ ,  $t_T$ ,  $t_F$ , and  $P$ ) using only the first four equations above (the three transit geometry equations and Kepler's Third Law with  $M_p \ll M_*$ ); this avoids any uncertainty from the stellar mass-radius relation.

The four combinations of parameters are: the planet-star radius ratio which trivially follows from equation (1),

$$\frac{R_p}{R_*} = \sqrt{\Delta F}; \quad (6)$$

the impact parameter  $b$ , defined as the projected distance between the planet and star centers during mid-transit in units of  $R_*$  (see Figure 1), and which can be derived directly from the transit shape equation (2), together with equation (6),

$$b \equiv \frac{a}{R_*} \cos i = \left[ \frac{(1 - \sqrt{\Delta F})^2 - \frac{\sin^2 \frac{t_F \pi}{P}}{\sin^2 \frac{t_T \pi}{P}} (1 + \sqrt{\Delta F})^2}{1 - \frac{\sin^2 \frac{t_F \pi}{P}}{\sin^2 \frac{t_T \pi}{P}}} \right]^{1/2}; \quad (7)$$

the ratio  $a/R_*$  which can be derived directly from the transit duration equation (3),

$$\frac{a}{R_*} = \left[ \frac{(1 + \sqrt{\Delta F})^2 - b^2 (1 - \sin^2 \frac{t_T \pi}{P})}{\sin^2 \frac{t_T \pi}{P}} \right]^{1/2}; \quad (8)$$

and the stellar density  $\rho_*$  which can be derived from the above equation for  $a/R_*$  and Kepler's Third Law with  $M_p \ll M_*$  (equation (4)),

$$\frac{\rho_*}{\rho_\odot} \equiv \frac{M_*/M_\odot}{(R_*/R_\odot)^3} = \left[ \frac{4\pi^2}{P^2 G} \right] \left[ \frac{(1 + \sqrt{\Delta F})^2 - b^2(1 - \sin^2 \frac{t_T \pi}{P})}{\sin^2 \frac{t_T \pi}{P}} \right]^{3/2}. \quad (9)$$

The parameters  $b$  and  $a/R_*$  are dimensionless. The density can also be written with the first term on the right hand side of equation (9) replaced by  $\frac{4\pi^2}{P^2 G} = \frac{365.25^2}{P^2 215^3}$ , with  $P$  in days.

It is interesting to consider the geometrical and physical origin of these combinations of parameters. The impact parameter  $b$  depends almost entirely on the transit shape (parameterized by  $t_F/t_T$ ) and ratio of planet and star sizes ( $\sqrt{\Delta F}$ ). To a lesser extent (cf. §3.3.2)  $b$  depends mildly on the period. The term  $a/R_*$  is the ratio of orbital distance to planet radius; to first order it is related to the ratio of transit duration to total period. The term  $a/R_*$  is also dependent on the impact parameter  $b$  and planet-star size ratio, because these parameters affect the transit duration. The stellar density,  $\rho_*$ , comes from Kepler's Third Law and the transit duration  $t_T$ ; Kepler's Third Law describes how much mass is enclosed inside the planet's orbit and the stellar radius is described by the transit duration with a physical scale set by Kepler's Third Law. Again,  $\rho_*$  is also dependent on the impact parameter  $b$  and the planet-star size ratio, because these parameters affect the transit duration.

### 3.2.2. The Five Physical Parameters

The five physical parameters  $R_*$ ,  $M_*$ ,  $i$ ,  $a$ , and  $R_p$  can be derived from the above solution for  $R_p/R_*$ ,  $b$ ,  $a/R_*$ , and  $\rho_*$  by using one additional equation: the stellar mass-radius relation (equation (5)). To derive  $M_*$ , consider equation (9) together with the stellar mass-radius relation in the form  $\rho_*/\rho_\odot \equiv M_*/M_\odot (R_*/R_\odot)^{-3} = (M_*/M_\odot)^{1-3x} 1/k^3$ :

$$\frac{M_*}{M_\odot} = \left[ k^3 \frac{\rho_*}{\rho_\odot} \right]^{\frac{1}{1-3x}}. \quad (10)$$

The stellar radius can be derived from the stellar mass by the stellar mass-radius relation, or from the density directly,

$$\frac{R_*}{R_\odot} = k \left( \frac{M_*}{M_\odot} \right)^x = \left[ k^{1/x} \frac{\rho_*}{\rho_\odot} \right]^{\frac{x}{(1-3x)}}; \quad (11)$$

the orbital radius  $a$  can be derived from  $M_*$  and from Kepler's third law with  $M_p \ll M_*$ ,

$$a = \left[ \frac{P^2 G M_*}{4\pi^2} \right]^{1/3}; \quad (12)$$

based on the definition of impact parameter (equation (7)), the orbital inclination is,

$$i = \cos^{-1} \left( b \frac{R_*}{a} \right), \quad (13)$$

and most importantly the planetary radius is

$$\frac{R_p}{R_\odot} = \frac{R_*}{R_\odot} \sqrt{\Delta F} = \left[ k^{1/x} \frac{\rho_*}{\rho_\odot} \right]^{\frac{x}{(1-3x)}} \sqrt{\Delta F}. \quad (14)$$

For main sequence stars  $k = 1$  and  $x \approx 0.8$ , in which case  $\frac{R_p}{R_\odot} = \left( \frac{\rho_*}{\rho_\odot} \right)^{-0.57} \sqrt{\Delta F}$ .

### 3.3. The Simplified Set of Equations and Their Solution

The equations and five-parameter solution take on a simpler form under the assumption  $R_* \ll a$ . This assumption is equivalent to  $t_T\pi/P \ll 1$  (from equation (8)), and has as its consequence  $\cos i \ll 1$  (from equation (13)). Systems we are interested in generally have  $t_T\pi/P < 0.15$  and likely  $t_T\pi/P \lesssim 0.1$  (or  $R_*/a \gtrsim 1/8$ ). Mathematically this assumption allows  $\arcsin x \approx x$  and  $\sin x \approx x$ . Under this approximation,  $\frac{\sin t_F\pi/P}{\sin t_T\pi/P} \approx t_F/t_T$ . A comparison of these two terms is shown Figure 2a; for cases of interest the terms agree to better than 4% and much better in most cases. Under the approximation  $t_T\pi/P \ll 1$ , a second term of interest,  $1 - \sin^2(t_T\pi/P) \approx 1$ . A comparison of this term as a function of  $t_T\pi/P$  (Figure 2b) shows agreement to better than 2.5% for cases of interest. The simplified solution will allow us to explore useful applications analytically in §6.

#### 3.3.1. The Simplified Equations

Under the approximations  $t_T\pi/P \ll 1$ , the transit shape (equation (2)) with  $\arcsin x \approx x$  becomes independent of  $P$ ,

$$\left(\frac{t_F}{t_T}\right)^2 = \frac{\left(1 - \frac{R_p}{R_*}\right)^2 - \left(\frac{a}{R_*} \cos i\right)^2}{\left(1 + \frac{R_p}{R_*}\right)^2 - \left(\frac{a}{R_*} \cos i\right)^2}, \quad (15)$$

and the total transit duration, (equation (3)), with  $\cos i \ll 1$  becomes

$$t_T = \frac{PR_*}{\pi a} \sqrt{\left(1 + \frac{R_p}{R_*}\right)^2 - \left(\frac{a}{R_*} \cos i\right)^2}. \quad (16)$$

The other three equations for transit depth (equation (1)), Kepler's Third Law (equation (4)), and the mass-radius relation (equation (5)), remain the same as in the exact solution. Note that by substituting  $b = \frac{a}{R_*} \cos i$  and  $\sqrt{\Delta F} = \frac{R_p}{R_*}$  the above equations take a very simple form.

#### 3.3.2. The Simplified Analytical Solution

The solution to the simplified equations is more useful than the exact solution for considering the general properties of light curves because  $P$  either cancels out of the solution or is a simple factor which can cancel out in parameter ratios. The impact parameter  $b$  (equation (7)), under the approximation  $t_T\pi/P \ll 1$ , becomes

$$b = \left[ \frac{(1 - \sqrt{\Delta F})^2 - \left(\frac{t_F}{t_T}\right)^2 (1 + \sqrt{\Delta F})^2}{1 - \left(\frac{t_F}{t_T}\right)^2} \right]^{1/2}; \quad (17)$$

the ratio  $a/R_*$  (equation (8)) becomes

$$\frac{a}{R_*} = \frac{2P}{\pi} \frac{\Delta F^{1/4}}{(t_T^2 - t_F^2)^{1/2}}; \quad (18)$$

and the stellar density  $\rho_*$  (equation (9)) becomes

$$\frac{\rho_*}{\rho_\odot} = \frac{32}{G\pi} P \frac{\Delta F^{3/4}}{(t_T^2 - t_F^2)^{3/2}}. \quad (19)$$

Note that for  $P, t_F$  and  $t_T$  in days, the first factor on the right side of equation (19) becomes  $32/G\pi = 3.46 \times 10^{-3}$ . The equation for  $R_p/R_*$  (equation (6)) clearly remains the same as in the non-simplified case. The stellar mass, stellar radius, orbital distance, orbital inclination, and planet radius can be derived as before with equations (10)–(14).

#### 4. Errors

In principle the unique solution of  $\rho_*$  and of the parameters  $M_*$ ,  $R_*$ ,  $i$ ,  $a$ , and  $R_p$  provides a powerful tool for understanding the transit light curve and more importantly for selecting the best transit candidates for radial velocity follow-up. In practice the usefulness of the unique solution is limited by errors caused by the limited photometric precision and time sampling of real data. The errors in the the star-planet parameters are very non-Gaussian and often correlated so a simulation is necessary in order to estimate errors. To compute the errors as a function of photometric precision and time sampling, we generated one thousand simulated transits with added Gaussian noise in the photometry for each of several combinations of photometric precision ( $\sigma$ ) and time sampling ( $\delta t$ ). We considered values of  $\sigma$  of 0.0025, 0.005, 0.01, and 0.015 mag and values of  $\delta t$  of 2.7, 6, and 12 minutes. Note that the shortest time sampling and highest photometric precision are reachable by current transit surveys (e.g., Mallén-Ornelas et al. 2002). We then fit the simulated transits for period, phase, depth, impact parameter, and stellar density with a  $\chi^2$  minimization fit. Additionally we solved for the planet radius using the main sequence stellar mass-radius relation with  $x = 0.8$ . For specificity we chose a star-planet model of  $P = 3.0$  days,  $M_* = M_\odot$ ,  $R_* = R_\odot$ ,  $\Delta F = 2\%$  (hence  $R_p = 0.14R_\odot = 1.45R_J$ ). Limb darkening was not included (see §5). We considered models with two different impact parameters ( $b = 0.2$  which corresponds to  $t_F/t_T = 0.74$  and  $b = 0.7$  which corresponds to  $t_F/t_T = 0.55$ ), because the errors are very sensitive to impact parameter of the input transit. Although for specificity we have focused on a single model (with two different impact parameters), for the purpose of error estimates changing  $t_T$  (by a change in  $P$ ,  $\Delta F$ ,  $a$ ; see equation (3) or (16) ) is equivalent to a linear change in time sampling, and changing  $\Delta F$  (by a change in  $R_p$  or  $R_*$ ; see equation (1)) is equivalent to a linear change in photometric precision. Thus errors in parameters from other models can be considered using the same computational results. Here we focus on the two most interesting parameters,  $\rho_*$  which can tell us if the star is on or close to the main sequence, and  $R_p$  an obvious quantity of interest for selecting the best planet candidates.

The errors in  $\rho_*$  and  $R_p$  are dominated by errors in the impact parameter  $b$ , which we discuss first. Figure 4 shows that for a given  $\Delta F$  there is a one-to-one correspondence between the impact parameter  $b$  and the transit shape as parameterized by  $t_F/t_T$ ; this one-to-one correspondence is one of the reasons for the existence of the unique solution. For “box-shaped” transits with large values of  $t_F/t_T$ , a small change in  $t_F/t_T$  can result in a very large change in  $b$ —making it difficult to derive  $b$  accurately from box-shaped transit light curves. This is not the case for transits with small  $t_F/t_T$  (i.e., with very long ingress/egress times), where  $b$  changes little even for a relatively large change in  $t_F/t_T$ . In the case of noisy data,  $b$  will be underestimated due to asymmetric errors resulting from the non-linear relation between  $b$  and  $t_F/t_T$ . An underestimate in  $b$  corresponds to an overestimate in  $\rho_*$  and an underestimate in  $R_*$  and  $R_p$ .

Figures 5, 6 and 7 show the errors in  $b$  and the fractional errors in  $\rho_*$  and  $R_p$  for the simulations on the specific transit model described above. Results for  $b = 0.2$  are shown on the left panels, and results for  $b = 0.7$  are shown on the right panels. The top and middle panels respectively show the rms and the median of the difference between the fit results and the input parameter (e.g., the rms and median of  $\{b_i - b_{model}\}$ , where the  $b_i$  are the fit results from each of the 1000 simulated noisy light curves, and  $b_{model}$

is the actual value used to create those light curves). The bottom panels show histograms of the fit results for each combination of photometric precision and time sampling. The vertical dotted lines indicate the correct value for the parameter in question (0.2 or 0.7 for  $b$ , and 0 in the case of fractional deviation for  $\rho_*$  and  $R_p$ ). From the median deviation plots and the histograms themselves, notice the severe systematic underestimate of  $b$  and the resulting over-estimate of  $\rho_*$  and  $R_p$  for cases with  $\sigma \gtrsim 0.005$  mag and  $b = 0.7$ . The rms fractional errors in  $\rho_*$  are 10% for  $b = 0.2$  and 20% for  $b = 0.7$  for a photometric precision of 0.0025 and a time sampling of 2.7 minutes. For this photometric precision and time sampling, the errors in  $R_p$  are less than 10% (neglecting uncertainty in the stellar mass-radius relation). The errors in  $R_p$  are  $\lesssim 40\%$  for time samplings  $\lesssim 6$  minutes and photometric precision  $\lesssim 0.005$ . These errors are quoted for the model used here, and as described above errors for models with different parameters (with the exception of changes in  $b$ ) can be derived by scaling  $\delta t$  and  $\sigma$  together with  $t_T$  and  $\Delta F$ . Note that folded transits from multiple low-time-sampled transit light curves can be used for higher effective time sampling and are useful as long as the photometric precision is high enough. A main point of these error simulations is that the transit shape must be well defined by high photometric precision and high time sampling, because most star-planet parameters depend on transit shape. Specifically a limiting factor is time sampling of ingress and egress and their start and end times to determine transit shape.

The errors for different combinations of photometric precision ( $\sigma$ ) and time sampling ( $\delta t$ ) are related because the total S/N per transit is based on both  $\sigma$  and  $\delta t$ . In particular the total number of photons per transit goes roughly as:

$$N_{\text{photons per transit}} \sim \left(\frac{t_T}{\delta t}\right) \left(\frac{1}{\sigma^2}\right). \quad (20)$$

It is interesting to note that our simulations show that the same error distribution will result from  $\delta t$  and  $\sigma$  combinations that give the same total number of photons per transit. E.g., compare the errors for a given  $\delta t$  and  $\sigma$  with those for  $\delta t \times 4$  and  $\sigma/2$ . This can be seen in Figure 7 where the same errors and error distribution results for  $\delta t = 12$  mins,  $\sigma = 0.0025$  mag and for  $\delta t = 2.7$  mins,  $\sigma = 0.005$  mag. Taking this into account, an optimal strategy of time sampling and exposure time can be chosen for a given mirror size and detector read time. Note that in practice,  $\delta t \ll t_T$  is required in order to reach reasonable errors in the derived parameters.

## 5. Limb Darkening

The transit light curve equations, their solution, and applications described in this paper assume no limb darkening. For the framework used in this paper,  $t_F$  (see Figure 1) must be measureable from the light curve—this is only possibly at wavelengths where limb darkening is weak. Figure 3 shows that  $t_F$  and  $t_T$  are distinguishable for measurements at  $I$ -band. At bluer band passes limb darkening becomes significant and it is not clear when the ingress/egress ends and begins and when the planet is fully superimposed on the star.

It is possible to incorporate limb darkening into the mathematical description of a planet transit light curve by parameterizing the transit shape by the slope of the ingress/egress instead of by  $t_F$  and  $t_T$ . The slope of ingress/egress is given by the time derivative of the transit area equation, including a parameterization for limb darkening. Figure 3 shows that the slope of ingress/egress is similar for a planet transit in different colors; the different slopes are generally equivalent within typical observational errors. This is because, for  $R_p \ll R_*$ , the ingress/egress slope is mainly due to the time it takes the planet to cross the stellar limb. In addition, the depth of the transit is affected by limb darkening. As a consequence of



these two additions the equations that describe the transit light curve take a cumbersome form and there is no longer a simple analytical solution. Of course a model fit with limb darkening can still be used to determine the parameters of the system. However, for a quick parameter estimate and the applications described in §6 an analytic solution is simple and practical; *I*-band or redder observations can be used to circumvent the complications of limb darkening.

## 6. Applications

The existence of a unique solution to a planet transit light curve has several applications. The first application is an analytic solution for planet-star parameters by using the equations in §3.2.2 with the values from §3.2.1 or §3.3.2. This analytical solution is useful for a quick parameter estimate. In this section we use the simplified analytic solution (§3.3) to explore the usefulness of four additional applications.

### 6.1. Measuring Stellar Density Directly from the Transit Light Curve

The density  $\rho_* = M_* R_*^{-3}$ , as described analytically in equations (9) and (19), is directly measurable from the light curve observables ( $\Delta F$ ,  $t_T$ ,  $t_F$ , and  $P$ ), together with Kepler’s Third Law. A measured density makes it possible to immediately distinguish between a main sequence star and a giant star from the transit light curve alone (i.e., without color data or spectra). Knowing the stellar size to first order immediately is useful for an estimate of  $R_p$  from the depth of the transit (equation (14)). For example, eclipses of  $\Delta F = 1\%$  for a giant star would be caused by a stellar companion, not a planetary companion. Figure 8 shows the density as a function of spectral type. A density measurement would give a position on the *y*-axis only. As shown by the box in Figure 8, F0V to M0V stars occupy a unique region of stellar density parameter space. Hence a density measurement can tell us that a given star is in the vicinity of main sequence stars. The main sequence stellar spectral type can be estimated for a given  $\rho_*$  by using the mass-radius relation for main sequence stars.

The stellar type (and hence  $R_*$  and  $R_p$ ) may not be identified with 100% certainty from  $\rho_*$  alone due to confusion with stars slightly evolved off of the main sequence; the unique density derivation clearly does not specify the actual stellar mass and radius. As main sequence stars begin to leave the main sequence they will evolve with constant mass to lower density as their radius increases (on vertical downward lines in Figure 8). These slightly evolved stars will fill in the box in Figure 8 to the lower left of the main sequence star diagonal line. Nevertheless, for a given  $\rho_*$  the corresponding  $R_*$  of a main-sequence star will always be the upper limit of  $R_*$ , whether or not the star is slightly evolved. Thus, we can always determine an upper limit to  $R_*$ —and hence to  $R_p$ —from  $\rho_*$  alone. Furthermore, a lower limit to  $R_*$  for a given  $\rho_*$  can be derived with the consideration that stars with  $M_* < 0.8M_\odot$  do not leave the main sequence in a Hubble time. Note that for densities corresponding F0V to M0V stars, the largest error in the radius estimation will occur for an evolved  $0.8M_\odot$  star with the density of an F0V star; in this extreme scenario, the radius over-estimate of the evolved star is only 25%. Beyond using the light curve alone, a derived surface gravity from a spectrum (measured to  $\lesssim 20\%$  precision for non-metal poor stars near the main sequence (Allende Prieto et al. 1999)) can be used with  $\rho_*$  derived from the transit light curve to determine  $M_*$  and  $R_*$ . Note that highly evolved stars will never be confused with main sequence or slightly evolved stars, since  $\rho_*$  will be significantly lower for highly evolved stars.

The errors for  $\rho_*$  are described in §4 and plotted in Figure 6. Figure 8 shows a plot of density vs. main

sequence spectral type, together with reference error bars. With an error in  $t_F$  and  $t_T$  of  $< 5$  minutes, and errors in  $\Delta F < 1\%$ , the stellar density can be constrained to 10%–20% depending on the transit shape (see §4). A consequence of the unique solution of  $\rho_*$  is that transit fitting codes which find equally good fits for different combinations of  $M_*$  and  $R_*$  actually find *the same*  $\rho_*$  for these best fits.

## 6.2. Contamination from Blended Stars: Transit Light Curve Alone

The five-parameter solution to a planet transit light curve with two or more transits is not unique if there is additional light from a blended star (or indeed if any of the assumptions in §2 are not fulfilled). A planet transit light curve can be mimicked by a stellar binary eclipsing system with contaminating light from a third, fully blended star. The additional light from the blended star causes an otherwise deep eclipse to appear shallow, and hence to mimic a planet transit light curve, as shown in Figure 9. This confusion is possible only when the eclipsing system has a flat-bottomed light curve, meaning that the eclipsing companion is fully superimposed on its primary star. Hereafter we call the eclipsing system plus the third fully blended star a “blend”.

### 6.2.1. Star-planet Parameters and Blends

The true, or actual, star-planet parameters will be confused by the contamination of blended light from an additional star. For selecting planet candidates for radial velocity follow-up it is useful to consider how some of the derived star and planet parameters change in the presence of blended light. In the following discussion we compare star and planet parameters naively derived from a transit light curve assuming no blend against those parameters derived by assuming the maximum possible amount of blended light.

The maximum amount of blended light for a given  $\Delta F$  is computed by considering the largest possible companion consistent with a given ingress/egress duration. This is equivalent to assuming a central transit (i.e.,  $b = 0$ ), and computing the maximum  $\Delta F$  possible for that given ingress/egress (i.e.,  $t_F/t_T$ ). Specifically, using  $b = 0$  in equation (15),

$$\Delta F_{b,real} \leq \Delta F_{b,real,max} = \frac{\left(1 - \frac{t_F}{t_T}\right)^2}{\left(1 + \frac{t_F}{t_T}\right)^2}. \quad (21)$$

Here the subscript  $b$  refers to a blend; the subscript  $obs$  refers to the eclipsing system parameters derived ignoring the presence of the third fully blended star whereas the subscript  $real$  refers to the actual parameters of the eclipsing binary. The subscript  $max$  refers to the quantities for the case of maximum possible blend (defined for a given  $t_F/t_T$ ).  $\Delta F_{b,obs}$  is the eclipse depth as taken from the observed light curve, and  $\Delta F_{b,real}$  is the actual eclipse depth (i.e., in the absence of the blended star). The ratio  $\Delta F_{b,real,max}/\Delta F_{b,obs}$  is shown in Figure 10a.

It is useful to consider the maximum difference between the density derived from a transit light curve in the presence of a blend ( $\rho_{b,obs}$ ) and the actual density of the eclipsed star ( $\rho_{b,real}$ ). We do this by using the simplified equation for  $\rho_*$  equation (19), to compute the ratio  $\rho_{b,obs}/\rho_{b,real,max}$ :

$$1 \leq \frac{\rho_{b,real}}{\rho_{b,obs}} \leq \frac{\rho_{b,real,max}}{\rho_{b,obs}} = \left[ \frac{\Delta F_{b,real,max}}{\Delta F_{b,obs}} \right]^{3/4}. \quad (22)$$

The stellar density is always underestimated from the light curve if a blend is present and ignored. A comparison of  $\rho_{b,real,max}$  and  $\rho_{b,obs}$  is shown in Figure 10b and is used in an application in subsection 6.3.

We can explore how the planet radius is affected by blends by considering how  $\rho_*$  is affected by blends (equation (22)) together with the simplified solution for planet radius, equation (14). The actual radius of the eclipsing companion,  $R_{p,b,real}$ , is related to the radius naively derived from the transit light curve ignoring the presence of a blend,  $R_{p,b,obs}$ , by

$$\frac{R_{p,b,real}}{R_{p,b,obs}} = \left[ \frac{\Delta F_{b,real}}{\Delta F_{b,obs}} \right]^{\frac{3x-2}{12x-4}} \leq \left[ \frac{\Delta F_{b,real,max}}{\Delta F_{b,obs}} \right]^{\frac{3x-2}{12x-4}}, \quad (23)$$

where  $x$  is the exponent in the stellar mass-radius relation (equation (5)). For main sequence stars,  $x \approx 0.8$  (Cox 2000) and the exponent in equation (23) becomes 0.071, so  $R_{p,b,real}/R_{p,b,obs}$  is mildly dependent on the amount of blended light present. The fact that there is a maximum value for  $\Delta F_{b,real}$  together with equation (23) implies that  $R_{p,b,real}$  also has a maximum for a given  $t_F/t_T$  and  $\Delta F$ . Figure 10c shows  $R_{p,b,real,max}/R_{p,b,obs}$  as a function of transit shape parameterized by  $t_F/t_T$ . In the presence of a blend, the actual radius of the eclipsing companion is always larger than the radius derived from the eclipsing light curve. Thus this figure shows the importance of ruling out blends—the eclipsing companion in a blended case could be larger than expected for a close-in planet ( $R_p \sim R_J$ ) by 20–50%.

### 6.2.2. Probability of Blends and Blend Limits

Transits with short ingress and egress times (box-shaped transits with large  $t_F/t_T$ ) are least likely to be affected by blended stars and can be the best planet transit candidates for follow-up radial velocity mass measurements. There are two reasons for this. First, less blended light can be hidden in a shallow transit with large  $t_F/t_T$  than one with small  $t_F/t_T$ . This is seen directly from the maximum value of  $\Delta F_{b,real,max}$  given in equation (21) and shown in Figure 10a.

The second reason why box-shaped transits are least likely to be affected by blended stars is because of the geometric probability for different transit shapes given random orientations of orbital inclinations. First it is useful to recognize that the unique solution to the planet-star parameters is in part possible because for a given  $\Delta F$  there is a one-to-one correspondence between the impact parameter  $b$  and the transit shape as parameterized by  $t_F/t_T$ . This  $b$  vs.  $t_F/t_T$  relation is non linear, as shown in Figure 4. For a random orientation of orbital inclinations, the cumulative probability  $P_c$  that an unblended transit will have impact parameter  $b$  smaller than some given value  $b_x$  is proportional to  $b_x$ ; the maximum value of  $b$  for a transit is  $1 - R_p/R_* = 1 - \sqrt{\Delta F}$ , where  $\sqrt{\Delta F}$  is the value for an unblended transit. Thus, the cumulative probability that an unblended transit will have  $b$  larger than  $b_x$  is described by

$$P_c(b \leq b_x) = \frac{1 - \sqrt{\Delta F} - b_x}{1 - \sqrt{\Delta F}}, \quad (24)$$

and is shown in Figure 11a. Because of the one-to-one correspondence between  $b$  and transit shape, we can also express the cumulative probability in terms of  $t_F/t_T$  (i.e., transit shape), shown in Figure 11b. The cumulative probability in equation (24) and Figure 11 can be used to show that for an ensemble of transits, there should be more “box-shaped” transits (large  $t_f/t_T$ ) than transits with very long ingress/egress times (small  $t_f/t_T$ ).

The S/N that must be reached to be able to completely rule out a possible blend can be determined from the maximum real eclipse depth  $\Delta F_{b,real,max}$ . The light from the eclipsing primary star is always less

than or equal to the total amount of light from the blended system, and has a minimum value given by the maximum blend:

$$1 \geq \frac{F_{primary}}{F_{b,total}} = \frac{\Delta F_{b,obs}}{\Delta F_{b,real}} \geq \frac{\Delta F_{b,obs}}{\Delta F_{b,real,max}}. \quad (25)$$

Thus, the quantity  $\Delta F_{b,obs}/\Delta F_{b,real,max}$  gives a lower limit to the fraction of the observed light which comes from the primary star in the eclipsing system. This can be used to establish the data quality necessary to find or rule out a blend in a given case. The light from the eclipsing primary in the blend could be detected, for example, by cross-correlating spectra of the blend with a suite of stellar templates to see if two cross-correlation peaks are present, or by resolving the blend with high spatial resolution imaging (e.g., from space or adaptive optics).

To summarize this subsection:

- box-shaped transits are the best planet candidates for radial velocity mass follow-up because (1) the least amount of blended light can be hidden in box-shaped transits and (2) for an ensemble of randomly oriented orbital inclinations there should be many more box-shaped transits with large  $t_F/t_T$  than transits with small  $t_F/t_T$ .
- In the presence of a blended star, the real planet radius is always larger than the naively derived planet radius ignoring the blend.
- The maximum brightness of a possible contaminating star can be derived from the transit light curve.

### 6.3. Contamination from Blended Stars: Transit Light Curve *and* a Known Spectral Type

Knowing the spectral type independently of the parameters derived from the transit light curve can be extremely useful in ruling out blends. With  $M_*$  and  $R_*$  determined from a spectral type, the system of equations (1)–(4) is overconstrained. If the stellar density  $\rho_{b,obs}$  as derived from the light curve from equation (9) is very different from the density  $\rho_{spect}$  of the observed spectral type then something is amiss with the light curve assumptions in §2. A possibility is the case of a blended star discussed above. Thus comparing  $\rho_{obs}$  with  $\rho_{spect}$  is extremely useful for detecting the presence of a blend.

For example the density can be overestimated a factor of up to 10 for  $t_F/t_T = 0.4$  and  $\Delta F = 0.1$ . The maximum density ratios on Figure 10b can be compared directly with the actual stellar main sequence densities shown in Figure 8. Furthermore, by comparing  $\rho_{obs}$  and  $\rho_{spect}$  we can detect the presence of a blend to an upper limit determined by the fractional errors in the stellar density,  $\frac{\delta\rho_*}{\rho_*} \simeq \sqrt{\left(\frac{\delta\rho_{obs}}{\rho_{obs}}\right)^2 + \left(\frac{\delta\rho_{spect}}{\rho_{spect}}\right)^2}$ . From equations (25) and (22) we can see that it will be possible to detect blends with  $\frac{F_{primary}}{F_{b,total}} = \frac{\Delta F_{b,obs}}{\Delta F_{b,real}} \gtrsim (1 - \frac{\delta\rho_*}{\rho_*})^{4/3}$ . Note that the error in  $\rho_{spect}$  must account for the fact that the spectrum may be dominated by the blended star, rather than by the primary star in the eclipsing system.

### 6.4. Blends and Statistics

Blended stars may be a common contaminant in transit searches (D. Latham, private communication 2001; Mallén-Ornelas et al., in preparation) either due to very wide binaries or, less likely in an uncrowded field, due to a chance alignment of a foreground or a background field star. In the presence of a third fully blended star some planet transits will be “washed out” and not detectable. Hence it is important to know

the blend frequency to determine the frequency of transiting planets. Even without a measured stellar spectral type, the frequency of blends contaminating the sample of planet candidates can be determined statistically by considering all of the flat-bottomed eclipses of various depths in the following way. Assuming the orbital inclination distribution is uniform, for a given  $\Delta F$  light curves should have a certain distribution of  $t_F/t_T$  (see the probability discussion in §6.2). Deviations from each expected distribution can be explained by eclipses being made more shallow than they should be by contaminating blended stars. The fraction of blended stars will also allow a statistical estimate of how many transits may be missed due to blends.

### 6.5. Period Derivation from Single-Transit Light Curves and a Known Spectral Type

The period can be estimated for a light curve with only one transit if  $M_*$  and  $R_*$  are known from a measured spectral type. Again, this is because the system of equations (1)–(4) that describe the transit light curve are overconstrained when  $M_*$  and  $R_*$  are known. Considering that  $M_*$  and  $R_*$  are known, and that the impact parameter is derived from equation (7), the period can be solved for from the following function of  $P$ :

$$\frac{4\pi^2}{P^2 G} \left[ \frac{(1 + \sqrt{\Delta F})^2 - b^2(1 - \sin^2 \frac{t_T \pi}{P})}{\sin^2 \frac{t_T \pi}{P}} \right]^{3/2} = \frac{M_*}{R_*^3}, \quad (26)$$

where the right hand side can be determined from the stellar spectral type. Under the approximation  $t_T \pi / P \ll 1$  the period is simply given by

$$P = \frac{M_* G \pi}{R_*^3 32} \frac{(t_T^2 - t_F^2)^{3/2}}{\Delta F^{3/4}}. \quad (27)$$

For  $P$  in days, the first term on the right hand side is  $\frac{G\pi}{32} = 288.73$ . The error for this  $P$  estimate is not easily derived because the errors in  $t_F$  and  $t_T$  are highly non-Gaussian and are often correlated. The fractional error in the period,  $\delta P/P$ , can be estimated for small errors in time sampling and photometric precision by noting that equation (27) is derived from the simplified equation for  $\rho_*$  (equation (19)), and that  $M_*$  and  $R_*$  would be known from the spectral type.  $\delta P/P = \sqrt{\left(\frac{\delta \rho_{obs}}{\rho_{obs}}\right)^2 + \left(\frac{\delta \rho_{spect}}{\rho_{spect}}\right)^2}$ , where  $\delta \rho_{obs}/\rho_{obs}$  is the fractional error in  $\rho_*$  derived from the transit light curve and  $\delta \rho_{spect}/\rho_{spect}$  is the fractional error in  $\rho_*$  derived from the spectral type. Thus, following the discussion in §4 and assuming  $\delta \rho_{spect}/\rho_{spect} \lesssim 0.1$ , the period can be determined to  $\sim 15$ – $20\%$  (depending on transit shape) for  $\delta t < 5$  minutes and  $\sigma \sim 0.0025$  mag.

An upper limit to the period can be estimated even without knowing  $t_F$ ,

$$P \leq \frac{G\pi M_*}{32 R_*^3} \frac{t_T^2}{\Delta F^{3/4}}. \quad (28)$$

This upper limit is valid even in the case of a blend where  $\Delta F_{b,real}$  is larger than the observed  $\Delta F$ .

## 7. Summary

We have presented the equations that describe a light curve with two or more transits and have presented the unique solution for the impact parameter  $b$ , the ratio of the orbital distance to stellar radius  $a/R_*$ , and stellar density  $\rho_*$ . Furthermore, with the stellar mass-radius relation we can uniquely derive the

five parameters  $M_*$ ,  $R_*$ ,  $i$ ,  $a$ ,  $R_p$ . This unique solution is only possible under the assumptions listed in §2, most importantly that the light curve is from a single star (i.e. not two or more fully blended stars), that the planet is dark and is in a circular orbit, and the light curve transits have flat bottoms (which can be obtained at red or longer wavelengths).

We have found:

- A simple analytical solution that can be used to quickly estimate the planet-star parameters, most importantly  $\rho_*$  and  $R_p$ ;
- The stellar density can be uniquely determined from the transit light curve alone. Fitting codes that solve for star-planet parameters will find a number of best fits for different combinations of  $M_*$  and  $R_*$ —these best fits will have the same stellar density.
- For noisy data, the impact parameter  $b$ ,  $R_*$  and  $R_p$  are underestimated and  $\rho_*$  is overestimated due to a non-linear one-to-one correspondence for a given  $\Delta F$  between  $b$  and transit shape (as parameterized by  $t_F/t_T$ ).

The existence of the unique solution for the above parameters allows several interesting applications, including:

- The stellar radius and the planet radius can be estimated based on  $\rho_*$ ;
- The likelihood that a shallow transit is due to contamination from a fully blended star can be estimated—with box-shaped transits being the least likely to be contaminated by blends;
- A comparison of  $\rho_*$  as determined from the transit light curve with  $\rho_*$  from a spectral type can help identify blended stars and hence indicate that shallow eclipses are not due to planet transits;
- In the presence of a blend the actual eclipsing companion radius is always larger than the radius derived from the light curve;
- The period from a single transit event can be estimated with a known spectral type.

For most of these applications time sampling of  $\delta t < 5$  minutes and photometric precision of  $\sigma < 0.005$  mag are needed (or more generally  $\sigma^2 \times \delta t \lesssim 1.5 \times 10^{-4} \text{ mag}^2 \text{ min}$ ). This time sampling and photometric precision is reachable with current planet transit surveys (e.g., Mallén-Ornelas et al. 2002). The transit shape must be well defined by high photometric precision and high time sampling because most star-planet parameters depend on transit shape. Specifically a limiting factor is time sampling of ingress and egress and their start and end times to determine transit shape.

We thank Howard Yee, Tim Brown, Scott Gaudi, and Gil Holder for useful discussions. S.S. is supported by the W.M. Keck Foundation. S.S. thanks John Bahcall for valuable advice, generous support, and encouragement. GMO thanks John Bahcall and the IAS for generous hospitality during visits when this work was carried out.

## REFERENCES

- Allende Prieto, C., López, G., Ramón, J., Lambert, D. L., & Gustafsson, B. 1999, ApJ, 527, 879  
 Borucki, W. J., Caldwell, D., Koch, D. G., & Webster, L. D. 2001, PASP, 113, 439  
 Brown, T. M., Charbonneau, D., Gilliland, R. L., Noyes, R. W., Burrows, A. 2001, ApJ, 552, 699  
 Charbonneau, D., Brown, T. M., Noyes, R. W., & Gilliland, R. L. 2002, ApJ, 568, 377

- Jenkins, J. M., Caldwell, D. A., Borucki, W. J. 2002 ApJ, 564, 495
- Mallén-Ornelas, G., Seager, S., Yee, H. K. C., Minniti, D., Gladders, M. D., Mallén-Fullerton, G., & Brown, T. M., submitted to ApJ, astro-ph/0203218
- Sackett, P. 1999, in Planets Outside the Solar System: Theory and Observations, eds. J.-M. Mariotti and D. Alloin, (Dordrecht: Kluwer), p.189-227
- Seager, S., & Hui, L. 2002, ApJ, in press, astro-ph/0204225
- Udalski, A. et al, 2002, Acta Astronomica submitted, astro-ph/0202320
- Zucker, S., & Mazeh, S. 2002, ApJ, 568, L113

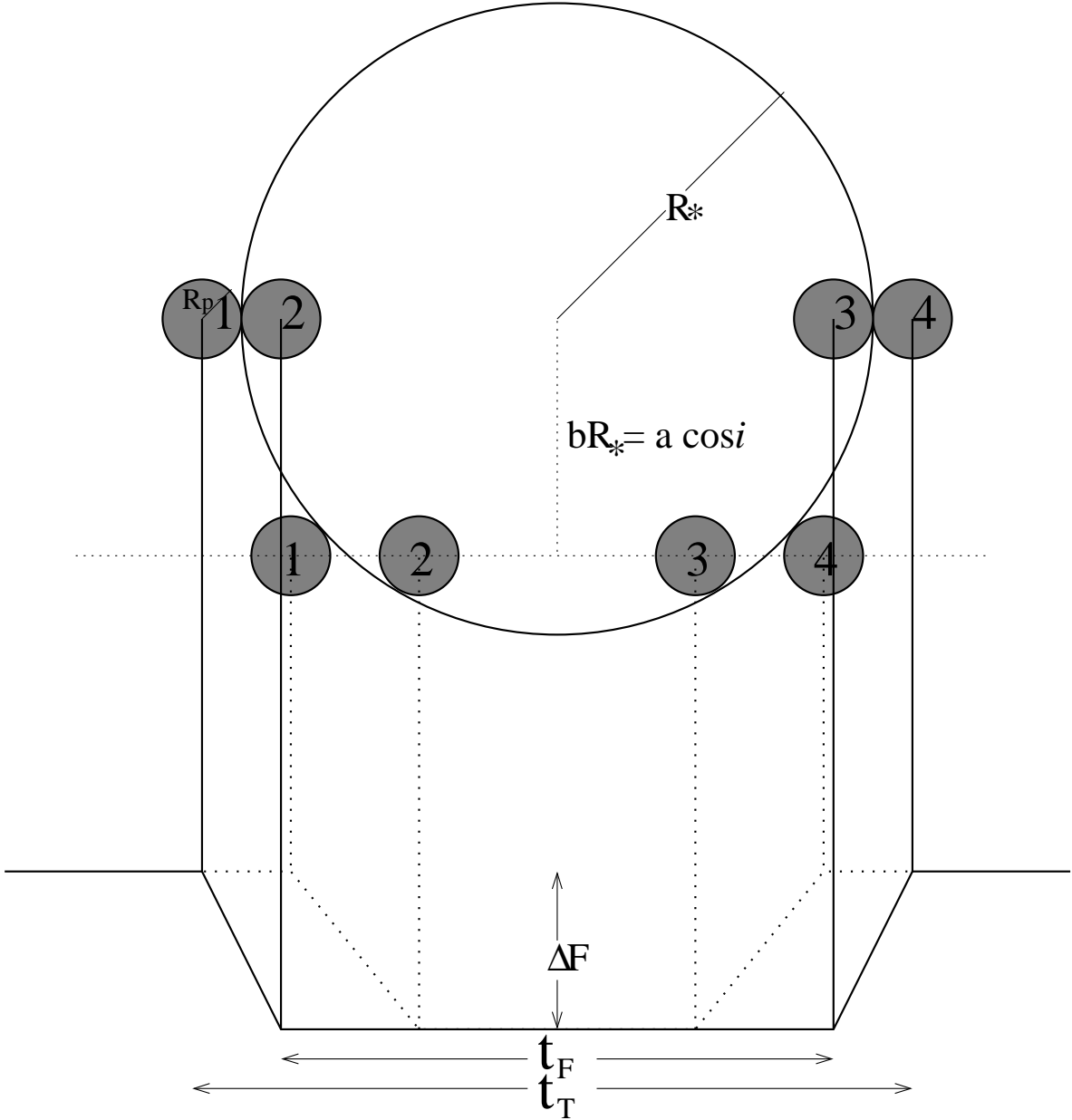


Fig. 1.— Definition of transit light curve observables. Two schematic light curves are shown on the bottom (solid and dotted lines), and the corresponding geometry of the star and planet is shown on the top. Indicated on the solid light curve are the transit depth,  $\Delta F$ ; the total transit duration,  $t_T$ ; and the transit duration between ingress and egress,  $t_F$ , (i.e., the “flat part” of the transit light curve when the planet is fully superimposed on the parent star). First, second, third, and fourth contacts are noted for a planet moving from left to right. Also defined are  $R_*$ ,  $R_p$ , and impact parameter  $b$  corresponding to orbital inclination  $i$ . Different impact parameters  $b$  (or different  $i$ ) will result in different transit shapes, as shown by the transits corresponding to the solid and dotted lines.



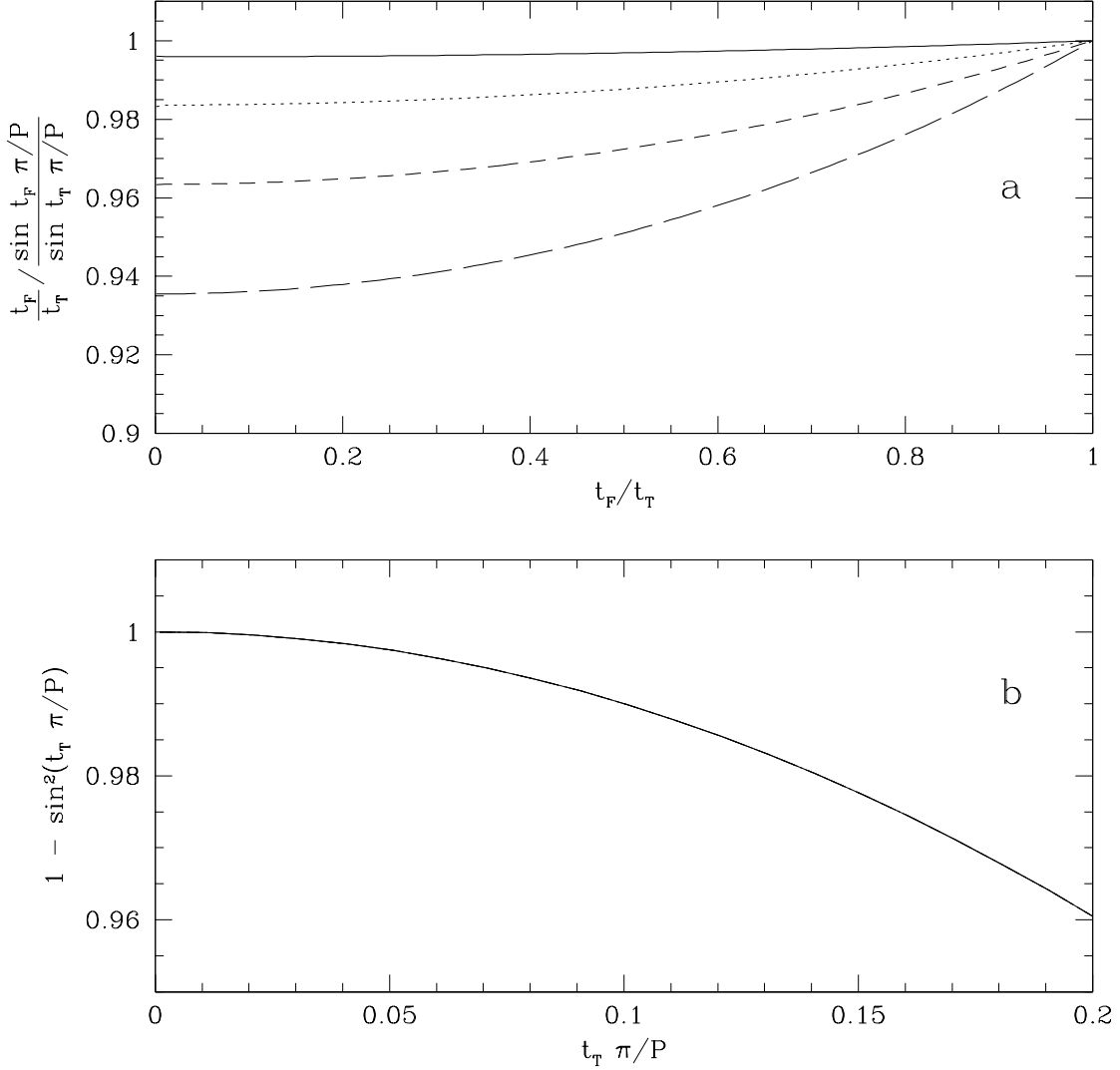


Fig. 2.— The validity of the approximation  $t_T P / \pi \ll 1$  (or equivalently  $R_* \ll a$ ). This approximation allows  $\sin t_T P / \pi \approx t_T P / \pi$ . Panel a: the term of interest  $\frac{\sin(t_F \pi / P)}{\sin(t_T \pi / P)}$  is reasonably well approximated by  $t_F / t_T$ . The different lines correspond to different values of  $t_T \pi / P$ : 0.05 (solid line), 0.1 (dotted line), 0.15 (short-dashed line), 0.2 (long dashed line). Panel b: the term of interest  $1 - \sin^2(t_T \pi / P)$  compared to its value, 1, under the approximation  $t_T P / \pi \ll 1$ . The short-period planet transit systems of interest will have  $t_T \pi / P < 0.15$  and usually  $t_T \pi / P \lesssim 0.1$ .

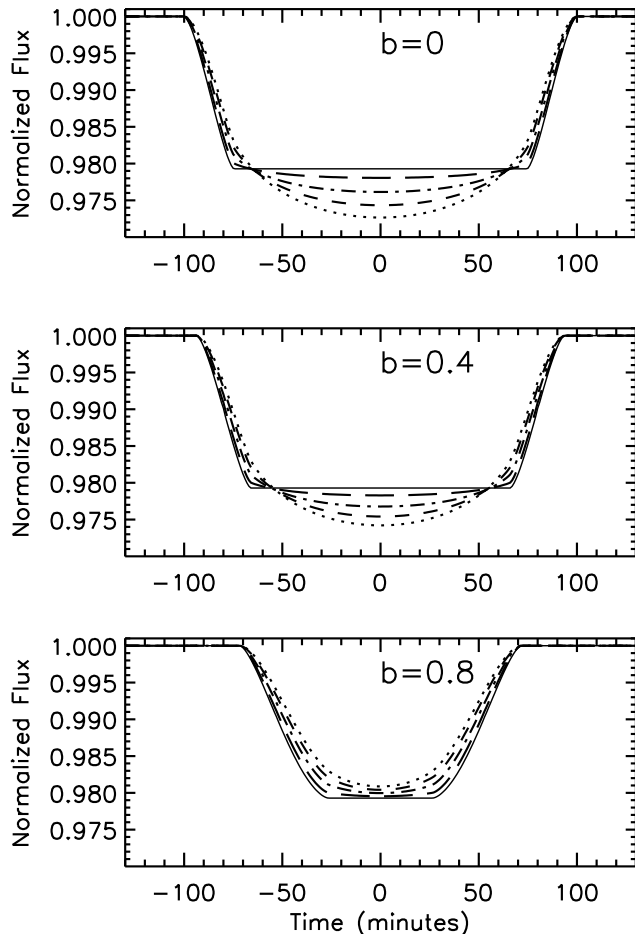


Fig. 3.— Solar limb darkening dependence of a planet transit light curve. In these theoretical light curves the planet has  $R_p = 1.4R_J$  and  $a = 0.05$  AU and the star has  $R_* = R_\odot$  and  $M_* = M_\odot$ . The solid curve shows a transit light curve with limb darkening neglected. The other planet transit light curves have solar limb darkening at wavelengths (in  $\mu\text{m}$ ): 3, 0.8, 0.55, 0.45. From top to bottom the panels show transits with different impact parameters  $b$ , which correspond to inclinations  $\cos i = bR_*/a$ . Although the transit depth changes at different wavelengths, the ingress and egress slope do not change significantly; the different slopes are generally equivalent within typical observational errors. The ingress and egress slope mainly depend on the time it takes the planet to cross the stellar limb.

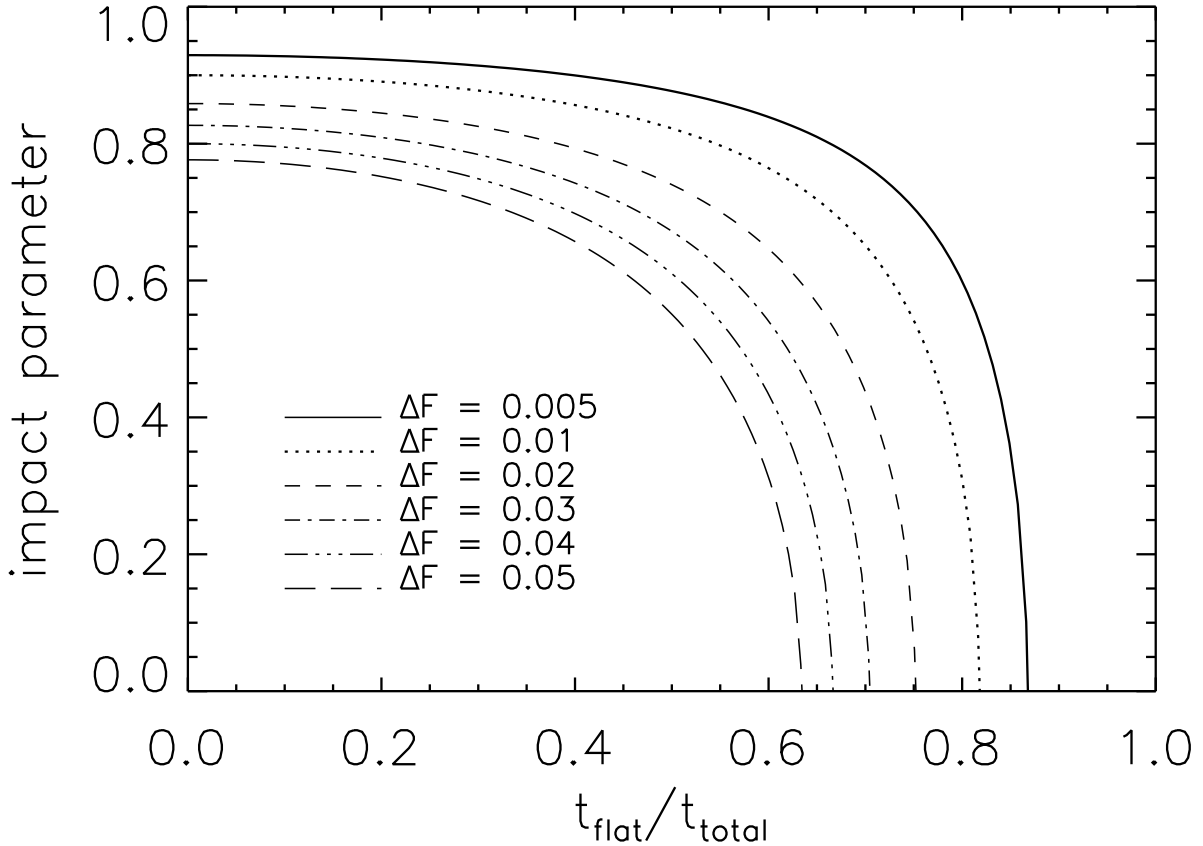


Fig. 4.— The one-to-one correspondence between the transit shape as parameterized by  $t_F/t_T$  and the impact parameter  $b$  for a given transit depth  $\Delta F$  (equation (17)). This one-to-one correspondence is one of the elements that makes the unique solution to the transit light curve possible. Transits with a given  $\Delta F$  can only fall along a given  $b$ - $t_F/t_T$  curve, and for a given  $\Delta F$  there is a maximum  $b$  and a corresponding minimum  $t_F/t_T$ . For large values of  $t_F/t_T$  (box shaped transits), a small change in  $t_F/t_T$  can result in a large change in  $b$ —making it difficult to derive  $b$  accurately from the transit light curve. This effect also causes an underestimate in  $b$  when the transit light curve is noisy, because a symmetric error in  $t_F/t_T$  causes a very asymmetric error in  $b$ .

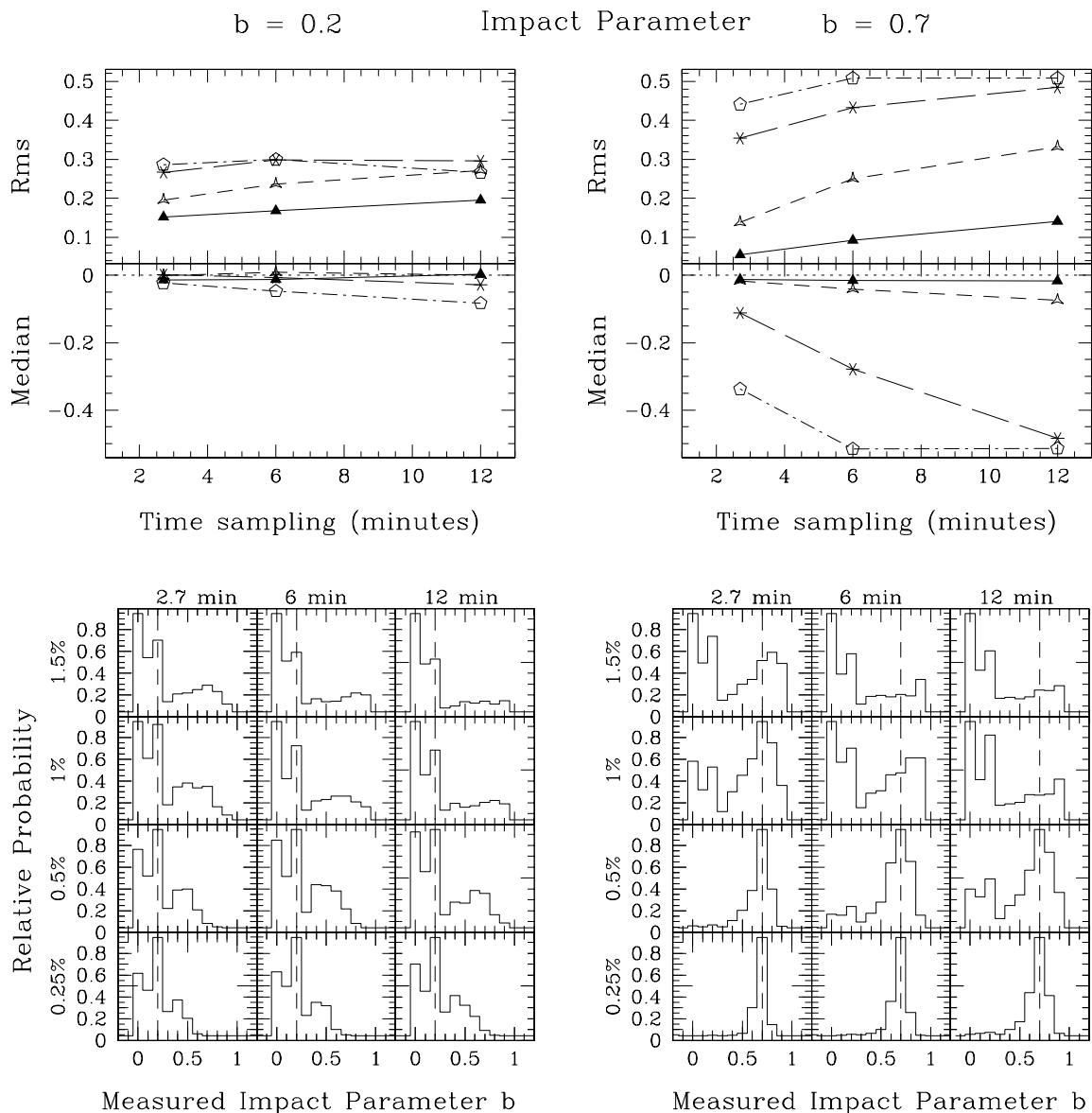


Fig. 5.— Errors in the derived impact parameter for the model  $P = 3.0$  days,  $M_* = M_\odot$ ,  $R_* = R_\odot$ ,  $\Delta F = 2\%$  (hence  $R_p = 0.14R_\odot = 1.45R_J$ ), and no limb darkening. The left panels are for  $b = 0.2$  and the right panels for  $b = 0.7$ . For each combination of photometric precision  $\sigma = 0.0025, 0.005, 0.01$  and  $0.015$  mag and time sampling  $\delta t = 2.7, 6$  and  $12$  min, 1000 noisy model transits were created and fit. The top panels show the rms of the difference between the measured and input  $b$ . The middle panels show the median of the difference between the measured and input  $b$  (an indication of systematic errors in the fits). The different curves are for different photometric precision  $\sigma = 0.015$  (pentagons),  $0.01$  (asterisks),  $0.005$  (open triangles),  $0.0025$  (solid triangles), and time sampling is shown in the  $x$ -axis. Notice the systematic under-estimate of  $b$ , especially evident for the  $b = 0.7$  models with large  $\sigma$  and  $\delta t$ . The bottom panels show normalized histograms of the of fit values for  $b$  for the different combinations of  $\delta t$  (increasing from left to right) and  $\sigma$  (increasing from bottom to top). The dotted line in each sub-panel indicates the input value for  $b$ . The figure shows that very high time sampling and high photometric precision are needed for a reasonably accurate fit ( $\lesssim 10$ – $20\%$  errors). When either the time sampling or photometric precision are very low, the value of  $b$  is consistently underestimated by the  $\chi^2$  fits (see text and Figure 4). The panels in this figure can be used to estimate errors in parameters from different models (for the same  $b$ ) by considering that changing  $t_T$  causes a linear change in time sampling and changing  $\Delta F$  causes a linear change in error in photometric precision. Note the trade off in  $\sigma$  vs.  $\delta t$ , where combinations with the same  $\sigma^2 \times \delta t$  have nearly identical error distributions.

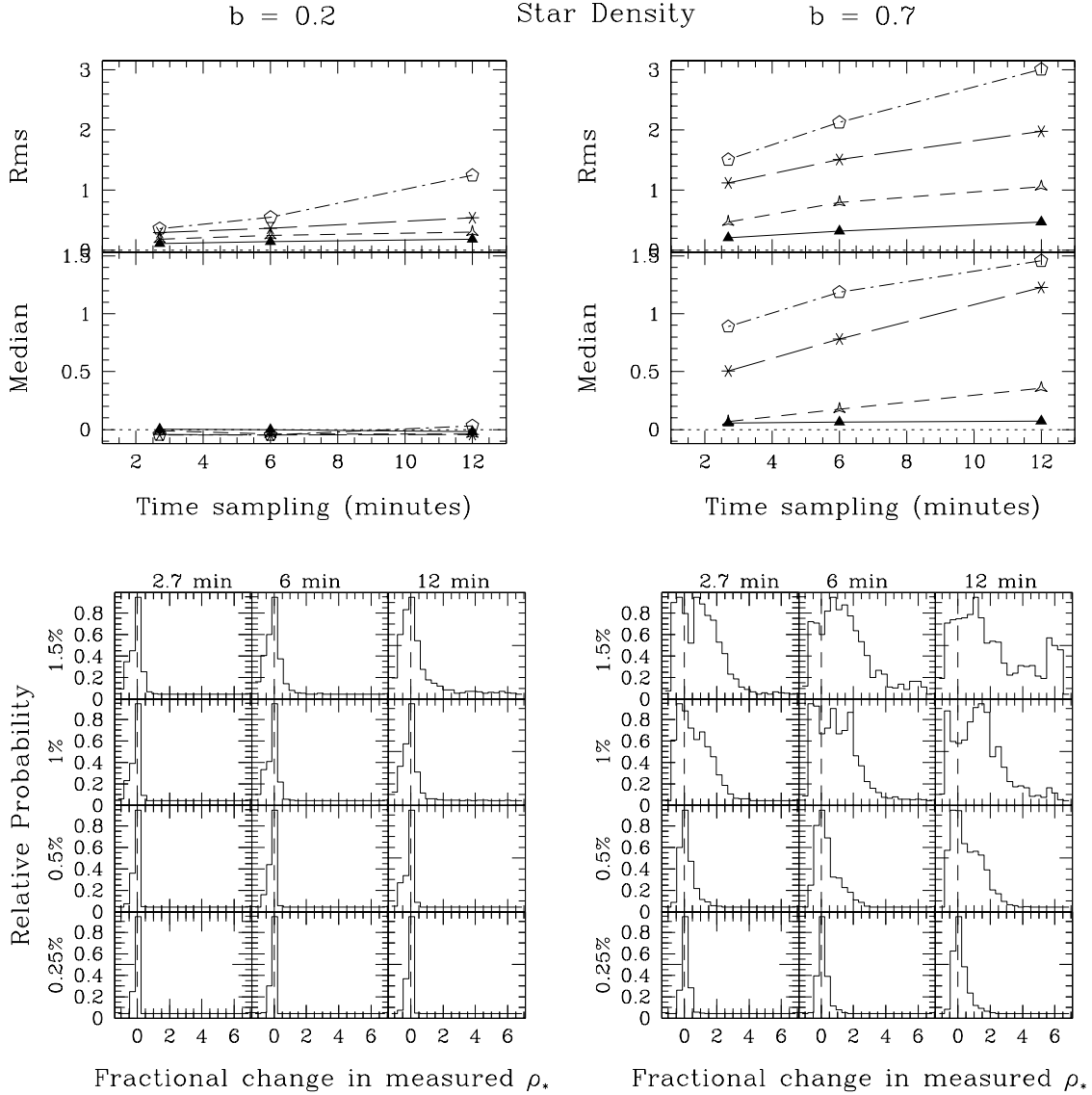


Fig. 6.— The fractional errors in the derived stellar density. See caption of Figure 5 for details. Notice that for low photometric precision and time sampling the density is significantly over-estimated for the  $b = 0.7$  case. This is a consequence of the under-estimate of  $b$  (see Figure 5).

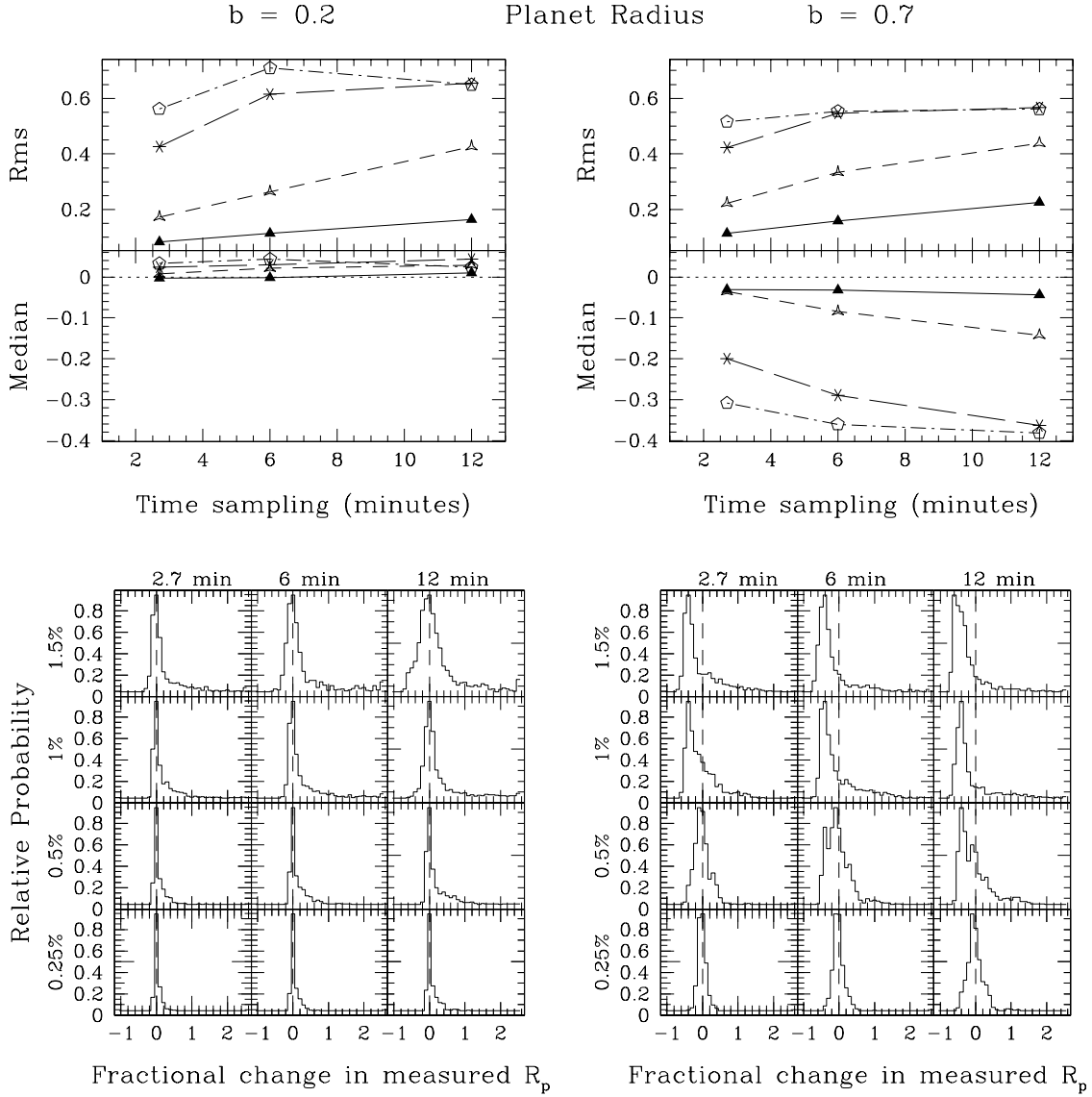


Fig. 7.— The fractional errors in the derived planet radius. See caption of Figure 5 for details. Notice that for low photometric precision and time sampling the planet radius is consistently under-estimated for the  $b = 0.7$  case. This is a consequence of the under-estimate of  $b$  (see Figure 5). This under-estimate will result in some M dwarfs being classified as planet-sized when using data with low photometric precision and time sampling.

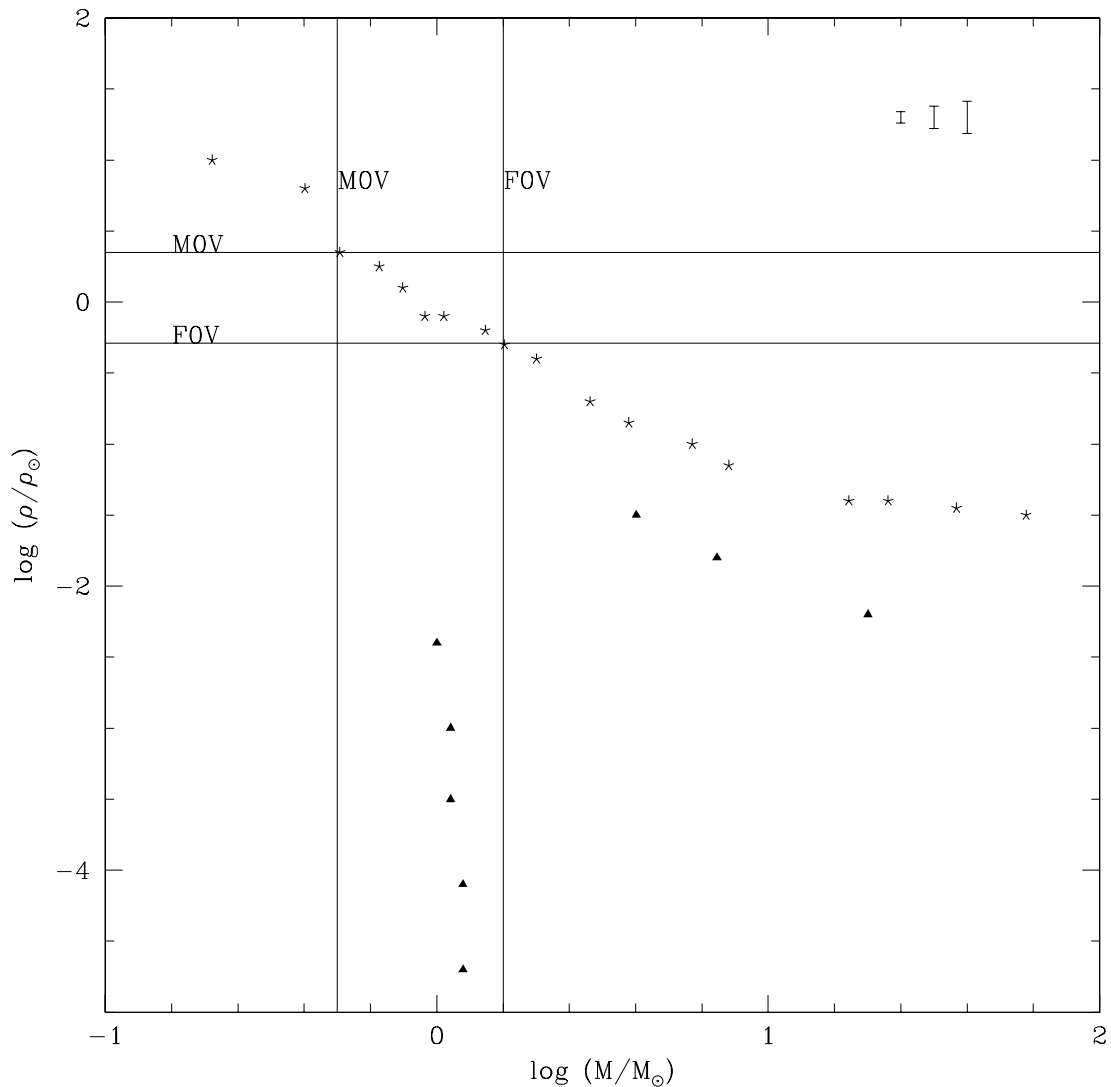


Fig. 8.— Stellar density  $\rho_*$  vs. star mass  $M_*$ . The asterisks show main sequence stars and the triangles show giant stars (Cox 2000). The unique solution of  $\rho_*$  from the planet transit light curves will give a position on the  $y$ -axis. The box MOV to F0V shows the main sequence stars which are most appropriate for finding transiting planets. These stars have a very different density from giant stars, and are therefore easily identifiable by their density alone. Although stars that have slightly evolved off of the main sequence will also populate the MOV/F0V box, their radii can still be estimated to  $\lesssim 25\%$  accuracy (see text). The error bars in the upper right corner are for fractional errors in  $\rho_*$  of 0.1, 0.2, and 0.3. See Figure 6 for the errors in  $\rho_*$ .

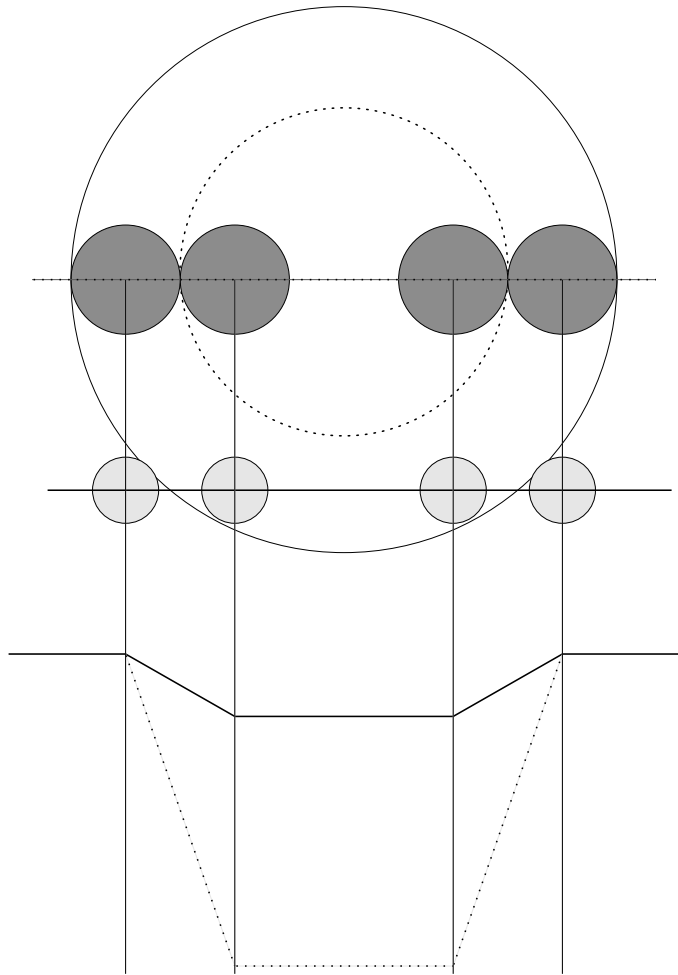


Fig. 9.— The effect of a blended star on a transit light curve. A schematic light curve (dotted line at the bottom) shows a relatively deep eclipse due to an eclipsing binary star system in which a small star centrally crosses the smaller primary star (dotted circle). In the presence of additional light from a third blended star (not shown), this deep eclipse will appear shallower, as shown by the solid line transit curve. This shallower solid-line transit looks the same as a planet transit crossing a larger star (solid line circle) with high impact parameter. Thus, there is no longer a unique solution to a transiting system in the presence of a blend. Note that any such blended transit will never look box-shaped, since the long ingress and egress are caused by the relatively long time it takes for the secondary star to cross the limb of the primary star.



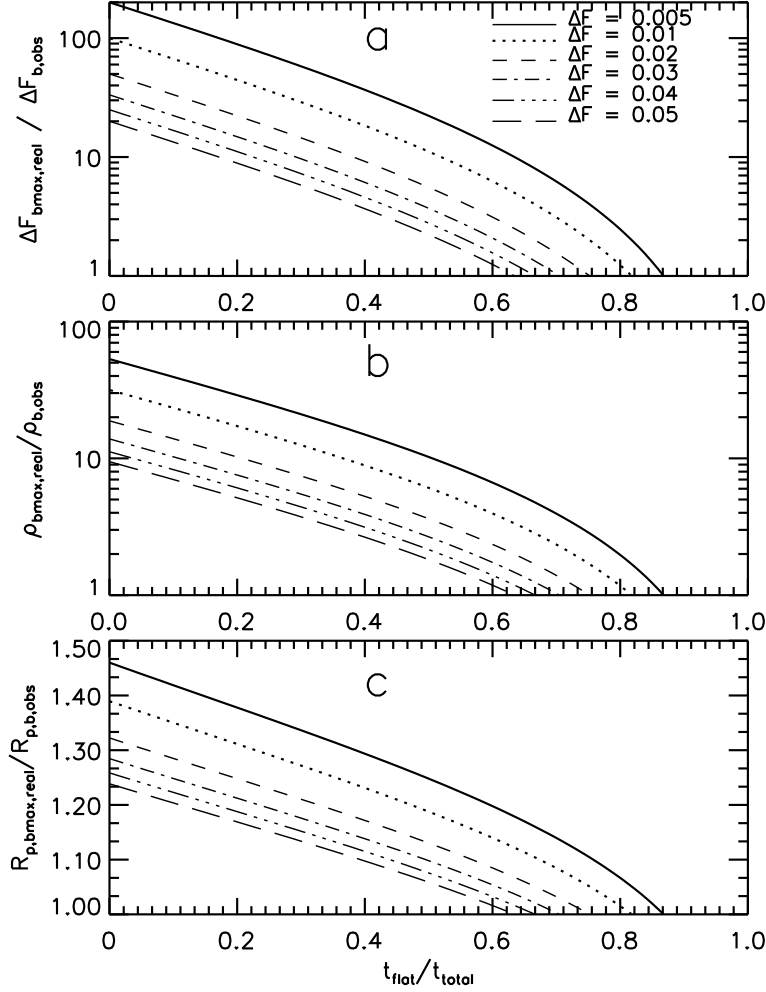


Fig. 10.— The maximum effect of a third fully blended star on the naively derived eclipsing system’s parameters  $\Delta F$ ,  $\rho_*$  and  $R_p$ . Panel a: The ratio between the maximum real eclipse depth in the presence of a blend  $\Delta F_{b,real,max}$  and the observed eclipse depth  $\Delta F_{b,obs}$  as a function of transit shape parameterized by  $t_F/t_T$  (see equation (21)). For a small transit depth (e.g.,  $\Delta F = 0.005$ ) and a small  $t_F/t_T$  (i.e., a nearly triangular transit shape) a large amount of extra light can be hidden in the transit light curve. Panel b: The ratio between the maximum real stellar density  $\rho_{b,real,max}$  and the naively-derived density  $\rho_{b,obs}$  in the case of a blend. This ratio depends on both  $t_F/t_T$  and  $\Delta F$  (equations (22) and (21)). Note that the real stellar density is always higher than the “observed” stellar density naively derived from a light curve ignoring the blend. Panel c: The ratio between the maximum real companion radius,  $R_{p,b,real,max}$  in the presence of a blend and the naively-derived radius  $R_{p,b,obs}$ , assuming the mass-radius relation for main sequence stars (see equation (23)). Note that in the case of a blend, the real eclipse depth, real stellar density, and real companion radius are always larger than the naively-derived observed values.

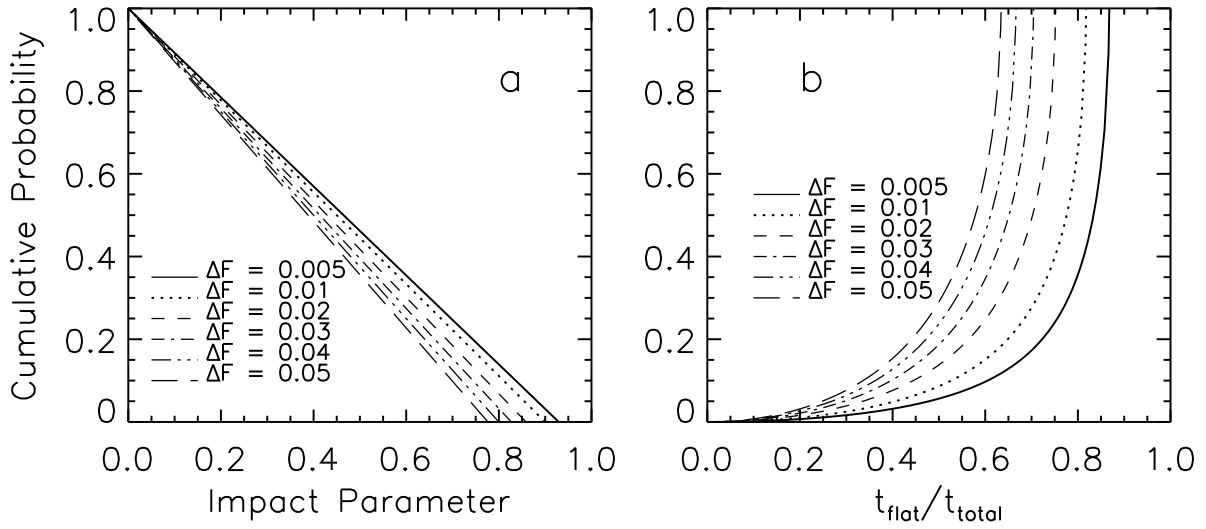


Fig. 11.— Panel a: the cumulative probability ( $P_c$ ) that, for a random orientation of orbital inclinations, a transit has impact parameter  $b$  which is *larger* than a specified impact parameter  $b_x$  (shown on the  $x$ -axis). This cumulative probability is just due to geometry. Panel b: the same cumulative probability as a function of transit shape, as parameterized by  $t_F/t_T$ .  $P_c$  can be described by both  $b$  and  $t_F/t_T$  because there is a one-to-one correspondence between them for a given transit depth, as shown in Figure 4. The  $P_c$  shows that “box-like” transit shapes (i.e., high  $t_F/t_T$ ) are much more common than transits with long ingress and egress (i.e., transits with small  $t_F/t_T$ ). If in a transit survey large fraction of transits of a given  $\Delta F$  are found to have small  $t_F/t_T$ , this is an indication that most of these systems are likely blended (see Figure 9).